processes

MDPI

Article

Evaluation of the Performance of a Combined Tillage Implement with Plough and Rotary Tiller by Experiment and DEM Simulation

Jun Du [1,2,*], Yifan Heng [1,2], Kan Zheng [1,2], Wenliang Zhang [1,2], Jumin Zhang [1,2] and Junfang Xia [1,2,*]

[1] College of Engineering, Huazhong Agricultural University, Wuhan 430070, China; hyf1003@webmail.hzau.edu.cn (Y.H.); zhengkan@mail.hzau.edu.cn (K.Z.); zhangwl940416@163.com (W.Z.); zjm@mail.hzau.edu.cn (J.Z.)

[2] Key Laboratory of Agricultural Equipment in Mid-Lower Yangtze River, Ministry of Agriculture, Wuhan 430070, China

* Correspondence: dujun@mail.hzau.edu.cn (J.D.); xjf@mail.hzau.edu.cn (J.X.); Tel.: +86-13296584073 (J.D.); +86-18694048763 (J.X.)

Abstract: In order to improve the performance of tillage tool for straw incorporation in silty clay loam, a combined tillage implement with plough and rotary tiller was designed. Its performance on straw incorporation and power consumption was investigated, and the combined tillage types (CTSR and CTDR) were compared with traditional tillage types including a sole plough type (SP and DP), a sole rotary tiller (RT), and a two-pass tillage type (SP+RT and DP+RT) in a rice field experiment. The effect of the forward speed and rotary speed for RT and CTSR were studied by DEM simulation. The ratio of straw coverage by CTSR and CTDR increased nearly 20% compared with RT, and the stability coefficient of tillage depth and CV of the surface evenness after tillage also improved in the field experiment. The total power of CTSR and CTDR was less than that of RT and two-pass tillage types by measurement. DEM simulation indicated that the total power of CTSR increased with the increase of the forward speed and rotary speed, and the reduction of the rotary power for the combined tillage implement can be obtained at a relatively high rotary speed. The combined tillage implement improved the performance on straw incorporation and had an advantage on power consumption at some operational conditions.

Keywords: DEM; tillage tools; straw incorporation; rotary tillage; simulation

Citation: Du, J.; Heng, Y.; Zheng, K.; Zhang, W.; Zhang, J.; Xia, J. Evaluation of the Performance of a Combined Tillage Implement with Plough and Rotary Tiller by Experiment and DEM Simulation. *Processes* **2021**, *9*, 1174. https://doi.org/10.3390/pr9071174

Academic Editors: Joanna Wiącek and David Fernández-Calviño

Received: 13 May 2021
Accepted: 2 July 2021
Published: 6 July 2021

1. Introduction

Soil tillage is the mechanical manipulation of the soil for different specific purposes and is one of the most important technological operations in agriculture. Studies around the world have shown that returning straw to the soil can significantly reduce greenhouse gas emissions, increase soil organic matter content, increase soil enzyme activity, improve soil aggregate structure, and increase crop yields [1]. Straw incorporation is the major practice of returning straw in a rice–rape cropping system in the middle and lower reaches of the Yangtze River [2].

The rotary tiller as an active tillage tool can be used to incorporate a range of surface applied materials into the soil and is widely used in the above region in China. The performance of a rotary tiller is affected by several geometrical and operational parameters such as the shape of blade, the working speed, and the rotary speed. The effects of rotary blade shape, rotational direction, number of rotary blades around the periphery, with and without soil-cutting disc blades on soil break up and torque requirements were investigated [3]. The computer graphics method was used to modify and develop rotary tiller blades [4]. It was observed that the blade required major rectification in its surface for the selected range of rotary speed, forward speed, and orientations. It was reported that the power consumption of a handheld tiller essentially depends on the geometric parameters

of rotary blades from a theoretical point of view [5]. Several studies investigated the effects of rotary blade geometry, operating speed, and cutting-edge geometry on the soil cutting and throwing process, torque and energy requirements, and furrow parameters in strip-tillage [6–8]. A full-scale rotary blade was tested in the field to investigate its mixing ability [9]. Soil cutting process was simulated by SPH and the Taguchi method to optimize the rotary blade. The bending point, alpha angle, and bending angle were considered as control factors, and power consumption was the evaluation index [10].

Several combined tillage implements combined multiple tillage tools, including active and passive or passive and passive tillage tool, gained popularity due to the reduced number of field trips and lower costs without sacrificing the quality of work. The rotary tiller is a popular tool of combined tillage implement, taking advantage of the forward thrust to help reduce draft. It was reported that taking advantage of negative draft of the active implement supplies a portion of the draft requirements of passive machine in a combined tillage tool [11]. The study revealed combining active and passive tillage elements leads to several benefits include the improvement of overall efficiency of the combined machine, stabilization of the working depth of the machine. A series of soil bin investigations on a laboratory prototype front active and rear passive set configuration of combined offset disc harrow (CODH) was conducted [12]. The CODH unites the benefits of powered discs and combination tillage with the aim to achieve timeliness in sowing, better crop residue handling with reduced tillage passes in rice-wheat cropping system, and improved engine power utilization of a tractor. The study revealed promising results with respect to significant reduction in draught force and superior tillage quality in terms of reduction in cone index of the tilled soil compared to the conventional free-rolling mode of offset disc harrow. The effect of velocity ratio on the performance of a combined offset disc harrow was investigated [13]. It indicated that increase in velocity ratio from 1.48 to 3.49 helped to reduce both draught and torque requirement, and those with negligible reduction observed when velocity ratio was increased beyond 3.49. A combined tillage implement consisting of two subsoiler shanks and a rotary harrow with four rotors was investigated in clay soil [14]. This implement reduced the draught of subsoiling by 4.4%–11.3% and required 10.5%–15.3% lower overall power compared to the combined power required by the subsoiler and rotary harrow working separately. A combined tillage implement of a subsoiler and a rotary harrow with two joints for two types of actual field conditions was developed to investigate tillage energy utilization and soil clod size [15]. The straw spatial distribution after straw incorporation by three types of tillage tools in rice stubble fields was compared [1]. The investigation revealed that the performance of SSR (combined tillage implement with subsoiling and special rotary blade) was more desirable than that of TR (traditional rotary blade) and SR (special rotary blade).

Discrete Element Method (DEM) was a promising method for soil-tool interaction studies and has been used in many tillage applications [16]. The full-scale rotary spader was tested using DEM and in the field, and proved that DEM can be used to model soil-rotary spader interaction to analyze different operation conditions [9]. The interaction between the soil and a moldboard plough was modelled by DEM, and the comparison with experimental test and analytical method proved that DEM has the potential to predict soil-moldboard plough interaction with a reasonable accuracy [17].

Since there are few studies on the combined tillage implement with plough and rotary tiller, the objective of this work was to evaluate the performance of a combined tillage implement on straw incorporation and power consumption in rice field compared with traditional tillage types. The performance indicators such as the ratio of straw coverage, stability coefficient of tillage depth and CV of surface evenness after tillage, and the force and power requirement were measured. The effect of operational parameters on the power consumption were analyzed by DEM simulation.

2. Materials and Methods

2.1. Description of the Test Site

Field experiments were conducted at the modern agricultural science and technology test base of Huazhong Agricultural University, Wuhan, Hubei province. The test site was a rice stubble field where there were amounts of anchored straw in the field. The straw stubble almost evenly covered the field. The soil type was silty clay loam (31 ± 2% clay, 63 ± 4% silt, and 6 ± 2% sand).

The physical properties of the soil and straw residue were measured before the experiment. The load of the straw per unit was the weight of straw in a 1 m square frame in the field. The height of the straw is defined as the length of the straw that stood upright in the field after harvest. It was determined by the average of 10 samples collected randomly obtained in the field. In our field, the load of the straw per unit was 1373.2 g/m^2, and the height of the straw was 461 mm.

All of the initial parameters of the soil were sampled by a five-point sampling method in the field. The soil cone index of the 0–100 mm and 100–200 mm layers was measured by cone penetrometer of TJSD-750 with 3 times for each test point and layer. The average value was taken as the soil cone index of that layer. The soil bulk density and moisture content were measured within depth 0–150 mm that was the main tillage depth. The original weight and the dried weight of the soil samples was measured to calculate the bulk density and the moisture content. The tested soil properties were listed in Table 1.

Table 1. Soil properties of the pre-tillage condition in the experiment field.

Parameter	Value
Cone index at depth of (kPa)	
0–100 mm	1409.6
100–200 mm	2731.7
Moisture content (%)	22.95
Bulk density (kg m^{-3})	1700

2.2. Tillage Tools and Operating Methods

In order to evaluate the performance of the combined tillage implement, several tillage types were compared in this work. These tillage types included a sole single-side plough (SP), a sole double-side plough (DP), a sole rotary tiller (RT), a two-pass tillage operation using a single-side plough followed by a rotary tiller (SP+RT), a two-pass tillage operation using a double-side plough followed by a rotary tiller (DP+RT), combined tillage implement with single-side plough and rotary tiller (CTSR), and combined tillage implement with double-side plough and rotary tiller (CTDR). In two-pass tillage type, there were two trips for tillage, and the soil was tilled by plough and rotary tiller successively.

Seven tillage types mentioned above were consisted of three tillage tools including single-side plough, double-side plough and rotary tiller as shown in Figure 1a–c. The key parameters of the single-side plough and double-side plough were their guide curves that consisted of curve height h, openness L, cutting edge ε, tangent angle ω, and starting segment s. The guide curve of the single-side plough and the double-side plough were shown in Figure 1d,e, respectively. The furrow width of the single-side plough and the double-side plough were 500 mm and 800 mm.

The rotary tiller consisted of blade shaft, rotary blade, spiral horizontal blade, machete, and cutter head. In the operation, the front rotary blades crush the soil and break the stubble, and the subsequent spiral horizontal blades press the straw to bury it. Finally, the straw is crushed and buried in the plough layer under the common kneading and stirring action of the rotary tiller and the spiral horizontal blades. The straw left on the surface is covered by the soil that thrown by the rotary tiller, and finally realize the operation of returning straw to the field. The working width of the whole blade roller was 2 m. The turning radius of the rotary tiller was 245 mm, and the turning radius of the spiral

horizontal blade was slightly less than that of the rotary tiller, which was 210 mm. The detail working principle of the rotary tiller has been introduced in our previous study [1].

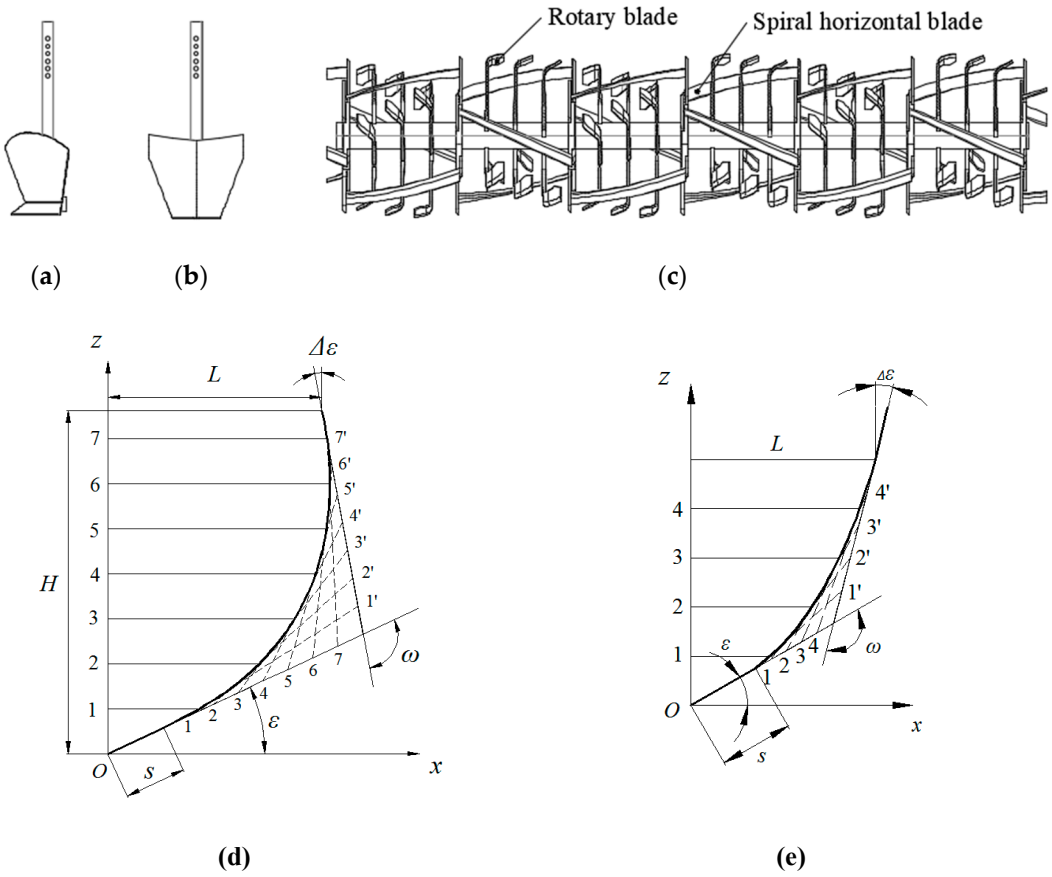

Figure 1. The schematic of the single-side plough, double-side plough and rotary tiller: (**a**) the single-side plough, (**b**) the double-side plough, (**c**) the rotary tiller, (**d**) the guide curve of the single-side plough, and (**e**) the guide curve of the double-side plough.

In the field experiment, one or two tillage tools were installed on the field experiment structure designed by our team, and the combined tillage implement for CTSR was shown in Figure 2. There were three ploughs at the front of the rotary tiller. The distance between ploughs was about 582 mm, and the distance between plough and rotary tiller was about 425 mm. For CTDR, the single-side plough was instead by the double-side plough. For SP, DP and RT, the corresponding plough or the rotary tiller was disassembled. The field experiment structure also included some other accessories such as furrow opener, weed cutter, depth roller, etc. The weight of the plough and the rotary tiller were 300 kg and 650 kg, respectively.

2.3. Eexperiment Design and Instrumentation

In order to compare the performance of different tillage types, the same operational parameters were set. Considering the field condition, the forward speed of the tractor was 0.43 m/s, while the rotary speed of the rotary tiller was 300 rpm. The tillage depth of the plough and rotary tiller was 180 mm to 220 mm and 140 mm to 180 mm, respectively. Draft power and rotary power were calculated by draught sensors and a torque sensor. The draught sensor was BK-5 with sensitivity of 1.5–2 mV/V and measuring range of 10 t. The torque sensor was CKY-810 with measuring range of 500 Nm and accuracy of ±0.5% FS. The data from the sensors was transmitted by its built-in wireless transmitter to the laptop computer.

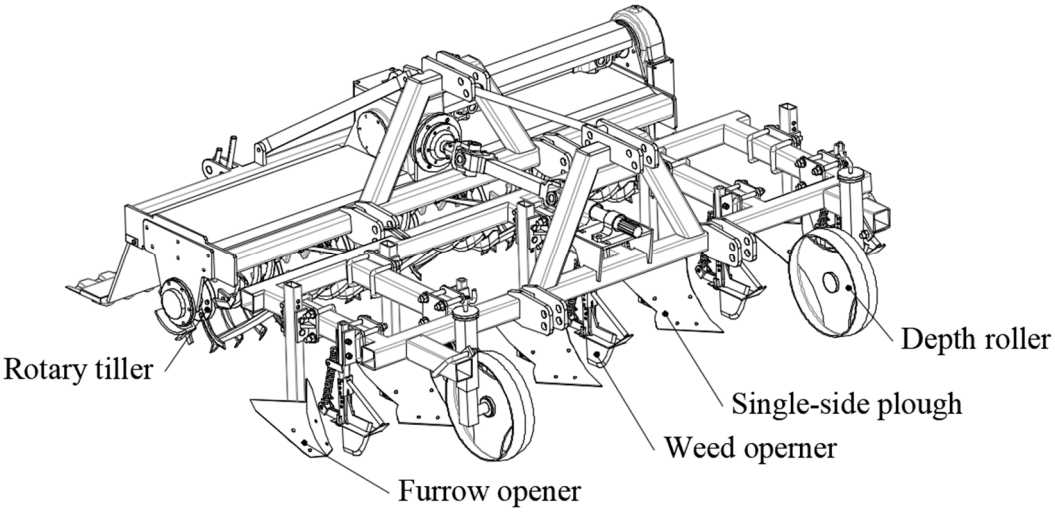

Figure 2. The schematic of the field experiment structure for CTSR.

In the field experiment, the tillage process of each tillage type (RT, SP+RT, DP+RT, CTSR, and CTDR) repeated 3 times. A total of 15 rice field plots were used in the field experiment. The width of each plot was 3 m to accommodate one pass of the field experiment structure. The length of each plot was 40 m, and the test length was 20 m located in the middle of the plot, as there were buffer areas at two ends of the plot for tractor acceleration and U-turn. A 70-kW tractor (LX954, YTO Agricultural Machinery Co., Ltd., Luoyang, China) was used as a traction tool for tillage.

2.4. Performance Characterization

2.4.1. Force and Power Requirement

The instrument system was set to measure the draft and vertical force, PTO torque, and PTO rotary speed. The draft power, the PTO power, and the total power were calculated by:

$$P_{total} = P_d + P_r \tag{1}$$

$$P_d = \frac{F_d v}{1000} \tag{2}$$

$$P_r = P_{PTO} = \frac{n_r M_r}{9550} \tag{3}$$

where P_{total} is the total power (kW), P_d and P_r are the draft power (kW) and the rotary power (kW), respectively. F_d is the draft force (kN) from the draught sensors, and v is the forward speed of the tillage implement (m/s). n_r is the PTO rotary speed (rpm), and M_r is the PTO torque (Nm) from the torque sensor. In this work, the rotary power was considered to be equal to the PTO power.

2.4.2. Ratio of Straw Coverage

The ratio of straw coverage was one of the most important performance indicators for a straw incorporation implement. The method for the ratio of straw coverage was followed Chinese national standard GB/T5668-2008. It was calculated according to the mass of the straw placed on the field surface pre- and after tillage. The mass of the straw on the field surface pre-tillage measured in Section 2.1. After tillage, a 1 m square frame was centered within the path of the tillage implement to obtain the straw placed on the field surface. The ratio of straw coverage was calculated by

$$R_c = \frac{m_o - m_t}{m_o} \times 100\% \tag{4}$$

where R_c is the ratio of straw coverage. m_o and m_t are the mass of the straw per unit placed on the field surface before and after tillage (kg), respectively.

2.4.3. Stability Coefficient of Tillage Depth

The stability coefficient of tillage depth represented the stability of the tillage depth, and it was given as follows:

$$SD_d = \sqrt{\frac{\sum_{i=1}^{n} (d_i - \overline{d})^2}{n-1}} \quad (5)$$

$$CV_d = \frac{SD_d}{\overline{d}} \quad (6)$$

$$S_d = (1 - CV_d) \times 100\% \quad (7)$$

where SD_d was the standard deviation of the tillage depth, and CV_d was the variation coefficient of the tillage depth. S_d was the stability coefficient of the tillage depth, and d_i was the tillage depth measured at plot i. $\overline{d}$ was the average tillage depth for a tillage type, and it was defined as

$$\overline{d} = \frac{\sum_{i=1}^{n} d_i}{n} \quad (8)$$

where n was the number of measurement plot of tillage depth for each tillage type. The tillage depth was measured at right and left side of tillage tool every 2 m along the forward direction. It meant that there were 20 data for each trip and 60 data for each tillage type.

2.4.4. CV of Surface Evenness after Tillage

CV of surface evenness after tillage was the deviation of the surface evenness after tillage, and it can be calculated by

$$CV = \sqrt{\frac{\sum_{i=1}^{n_s} (h_i - \overline{h})^2}{n_s - 1}} \quad (9)$$

where CV_{se} was the variable coefficient of the surface evenness after tillage, and n_s was the number of measurement plot of surface evenness after tillage for each tillage type. h_i was the height of the surface soil measured at plot i, and $\overline{h}$ was the average of the height of the surface soil. The height of the surface soil was measured within tillage width, and there were 10 measurement plots for each tillage width sample. A total of 3 tillage width samples were selected for each tillage type.

2.5. Simulation Model and Condition

2.5.1. Simulation Model

A cohesion contact model called Hertz–Mindlin with JKR model [18] was suggested to model the interaction between soil and soil in this study. It was based on the Johnson–Kendall–Roberts theory, and introduced a pull-off force to account for attractive forces between particles. Therefore, it allowed to model strongly adhesive systems. The detail of Hertz–Mindlin with JKR model was given by

$$f_c^n = -4\sqrt{\pi\gamma E^*}a^{3/2} + \frac{4E^*}{3R^*}a^3 \quad (10)$$

$$\delta_n = \frac{a^2}{R^*} - \sqrt{4\pi\gamma a / E^*} \quad (11)$$

where γ is the surface energy (J/m^2). a is the contact radius (mm), and δ_n is the normal overlap (mm). E^* and R^* are equivalent Young's modulus (Pa) and equivalent radius (mm), respectively, defined as,

$$\frac{1}{E^*} = \frac{1-\nu_i^2}{E_i} + \frac{1-\nu_j^2}{E_j} \tag{12}$$

$$\frac{1}{R^*} = \frac{1}{R_i} + \frac{1}{R_j} \tag{13}$$

where E_i, R_i, m_i and ν_i are the Young's Modulus, radius, mass, and Poisson ratio of particle i, respectively.

The tangential elastic contact force, the normal dissipation force and the tangential dissipation force in Hertz–Mindlin with JKR model used the same calculations as the Hertz–Minidlin contact model. They were given as,

$$f_c^t = S_t \delta_t \tag{14}$$

$$f_d^n = -2\sqrt{\frac{5}{6}}\beta\sqrt{S_n m^*}v_n^{rel} \tag{15}$$

$$f_{d,ij}^t = -2\sqrt{\frac{5}{6}}\beta\sqrt{S_t m^*}v_t^{rel} \tag{16}$$

where n and t represent the normal and tangential component of the contact force and the dissipation force. δ_t is the tangential components of particle overlap. v_n^{rel} and v_t^{rel} are the normal and tangential components of the relative velocity. The equations for β, the normal and tangential stiffness are given as follows:

$$\beta = \frac{\ln e}{\sqrt{\ln^2 e + \pi^2}} \tag{17}$$

$$S_n = 2E^*\sqrt{R^*\delta_n} \tag{18}$$

$$S_t = 8G^*\sqrt{R^*\delta_n} \tag{19}$$

where e is the coefficient of restitution, and the equivalent Shear modulus G^* is calculated by

$$\frac{1}{G^*} = \frac{2-\nu_i}{G_i} + \frac{2-\nu_j}{G_j} \tag{20}$$

The Young's modulus can be calculated by

$$G_i = \frac{E_i}{2(1+\nu_i)} \tag{21}$$

The detail governing equations of Hertz–Mindlin with JKR model are described in [19].

2.5.2. Simulation Condition

A domain of size 3500 × 2800 × 300 mm (width, length, height) was chosen to be the simulation soil bin based on the computation power of the computer and the size of tillage implement. The simulation soil bin allowed different tillage types to reach a stable condition in terms of the force and torque. The diameter of soil particle was 20 mm, and similar particle sizes had been used in the literature for the simulation of soil–tool interaction. The DEM input parameters were shown in Table 2. The density of soil particle was calculated according to the measurement of bulk density. Density of steel, Shear modulus of soil and steel, Poisson ration of soil and steel was referred to our previous studies. Coefficient of restitution of soil–soil and soil–steel, coefficient of static friction and rolling friction was referred to in the literature [20] because of a similar soil condition. The

soil surface energy for JKR model regarded as an important parameter was calibrated by the method mentioned in the literature [21], and 350 J/m^2 was set in this work.

Table 2. DEM input parameters used in the simulations.

Property	Value
Density of soil particle (kg m^{-3})	2644
Density of steel (kg m^{-3})	7860
Shear modulus of soil (Pa)	1.86×10^6
Shear modulus of steel (Pa)	7.90×10^{10}
Poisson ratio of soil (-)	0.37
Poisson ratio of steel (-)	0.30
Coefficient of restitution of soil–soil (-)	0.6
Coefficient of restitution of soil–steel (-)	0.6
Coefficient of static friction of soil–soil (-)	0.6
Coefficient of static friction of soil–steel (-)	0.6
Coefficient of rolling friction of soil–soil (-)	0.1
Coefficient of rolling friction of soil–steel (-)	0.1

The DEM simulation was implemented by EDEM 2018. The simplified solid assembly model of different tillage types was established with a 1:1 ratio and was imported into the EDEM software. The simplified solid assembly model for CTSR was illustrated in Figure 3. Considering the computation consumption, the straw was ignored in the simulation. For the calibration and validation cases, the operational condition kept the same as the actual field experiment. The forward speed was 0.43 m/s, and the rotary speed of rotary tiller was 300 rpm. In order to investigate the effect of the forward speed and the rotary speed on the force and power requirement, different operational parameters were conducted in the simulation.

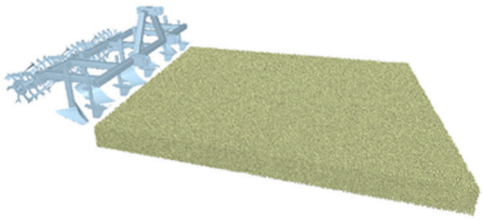

Figure 3. The simulation process of CTSR.

3. Results

3.1. Performance Indicators in the Field Experiment

The tillage processes of RT, CTSR, and CTDR were shown in Figure 4 and the performance indicators of RT, CTSR, and CTDR in the rice field experiment was given in Table 3. The ratio of straw coverage was an important performance indicator for straw incorporation tillage implement. The ratio of straw coverage of CTSR and CTDR was 89.84% and 90.53%, respectively, and increased obviously compared with that of RT, which was 68.95%. The stability coefficient of tillage depth of combined tillage implement was also higher than that of sole rotary tiller. It was observed that stability coefficient of tillage depth raised from 84.66% for RT to 88.50% for CTSR and 93.8% for CTDR. The performance of CTDR on the stability coefficient of tillage depth was better than CTSR. The value of CV of the surface evenness after tillage for CTSR and CTDR was approached to nearly 20 mm from 24.6 mm that obtained from RT. Compared with RT, CTSR, and CTDR increased the ratio of straw coverage and CV of tillage depth, and reduced the surface evenness after tillage in the rice field. It indicated that the combined tillage implement improved the performance of straw incorporation. CTSR and CTDR had different plough components. Their ratio of straw coverage and surface evenness after tillage were approximate, but CTDR presented a better performance on the stability coefficient of tillage depth.

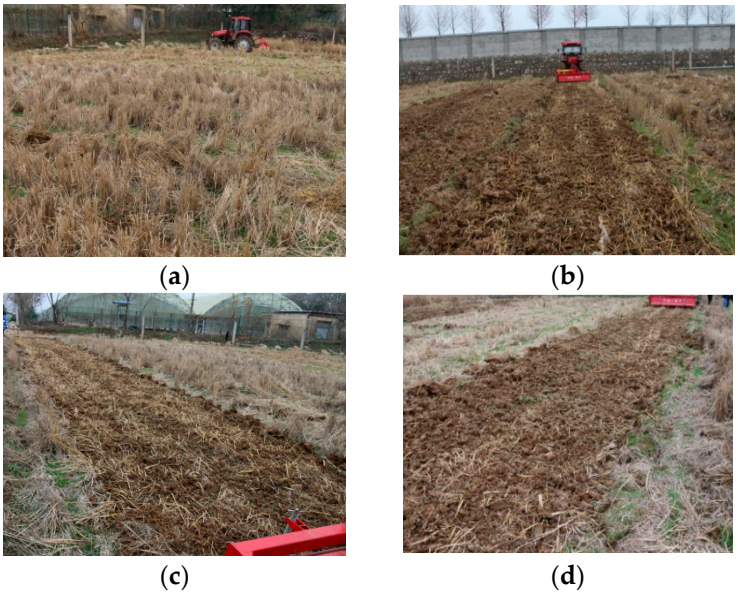

Figure 4. The tillage process of different tillage types: (**a**) Pre-tillage, (**b**) RT, (**c**) CTSR, and (**d**) CTDR.

Table 3. Performance indicators of different tillage types in the rice field experiment.

Tillage Type	Ratio of Straw Coverage (%)	Stability Coefficient of Tillage Depth (%)	CV of the Surface Evenness after Tillage (cm)
RT	68.95	84.66	2.46
CTSR	89.84	88.50	1.90
CTDR	90.53	93.8	2.00

3.2. Force and Power Requirement in the Field Experiment

The draft and vertical force of different tillage type in the rice field experiment was shown in Figure 5. The draft force of SP, DP, RT, CTSR, and CTDR were obtained from sensors directly, while the draft force of two-pass tillage type (SP+RT and DP+RT) was the total draft force from each pass which means the sum of the draft force from plough tillage and rotary tillage. As the RT was an active tillage operation, its draft force was dramatically less than others. The two-pass tillage type obtained the largest draft force. For SP+RT, the draft force from SP was only 13.68 kN, which was 84.77% of the total draft force. The DR+RT can obtain a similar percentage. It found that the draft force from plough tillage was the majority part of the draft force for two-pass tillage type. The draft force of CTSR and CTDR were 15.72 kN and 17.32 kN, respectively. They were larger than that of sole plough tillage type (SP and DP), but less than that of two-pass tillage type. The vertical force of SP and DP was −2.69 kN and −2.93 kN, respectively. Contrary to RT, CTSR, and CTDR, the vertical force of SP and DP were negative that meant their direction was pointed to the ground. Moreover, the value of the vertical force of CTSR and CTDR was less than that of RT. It demonstrated that the plough component can make the tillage depth stable.

The power requirement of different tillage types in rice field experiment were given in Figure 6. The total power was the sum of the draft power and the rotary power. In the rice field experiment, the rotary power contributed the vast majority of the total power. The total power of RT was 49.81 kW, while the rotary power of RT was 48.72 kW, which was 97.81% of the total power. The percentage of the rotary power to the total power for SP+RT, DP+RT, CTSR, and CTDR were more than 80%. The two-pass tillage types obtained the largest total power, as they had a relatively larger draft power. The draft power of SP+RT and DP+RT was obtained from both trips, while the rotary power was obtained from their second pass with rotary tillage. The rotary power of SP+RT and DP+RT were 48.27 kW and 48.22 kW, respectively, that were similar with the rotary power of RT. However, the total

draft power of SP+RT and DP+RT raised to 6.94 kW and 8.16 kW that dramatically larger than the draft power of RT. The combined tillage types required the least total power, and the total power of CTSR and CTDR were 42.32 kW and 46.26 kW, respectively. CTSR and CTDR had the largest draft power. However, the proportion of the draft power on the total power was low, and there was a significant reduction on the rotary power for CTSR and CTDR. The rotary power of CTSR and CTDR were 35.56 kW and 38.81 kW that decreased nearly 20%. It indicated the advantage of the combined tillage type on power consumption.

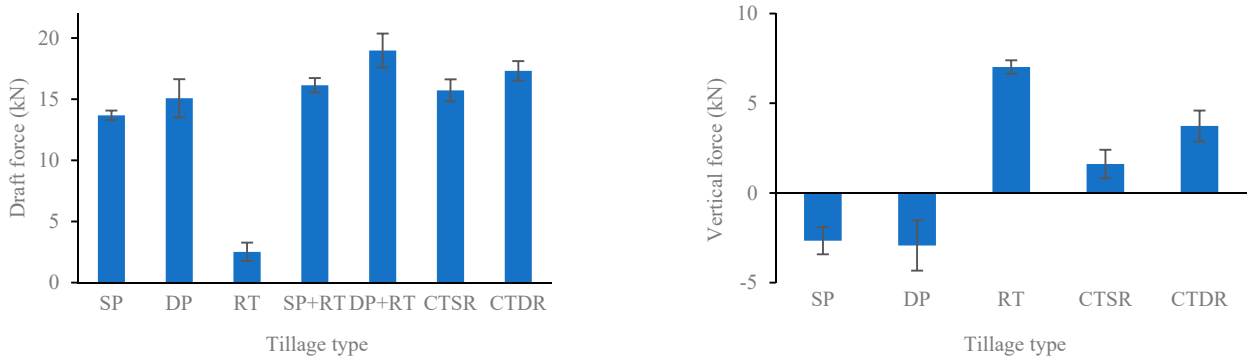

Figure 5. The draft and vertical forces of different tillage types: (**a**) draft force and (**b**) vertical force. (Bar graph represents the mean value, and error bars represent standard deviations).

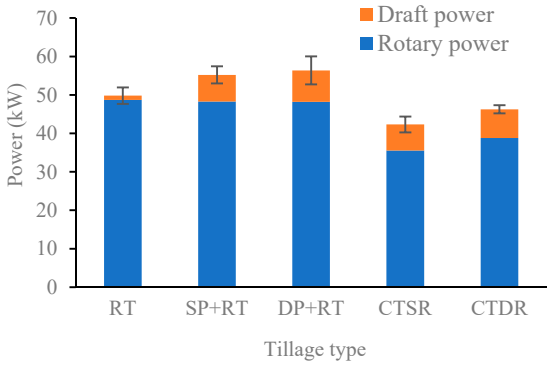

Figure 6. Power characteristics of different tillage type in the rice field experiment. (Bar graph represents the mean value, and error bars represent standard deviations).

3.3. The Effect of Working Conditions on Power Consumption in Simulation

The effect of the forward speed and rotary speed on the force and power of a combined tillage implement was investigated by DEM simulation in this section. As the rotary power was the majority of the total power, the DEM model was validated based on the rotary power of RT. In the validation case, the operational parameters kept the same with the field experiment. The forward speed was 0.43 m/s and the rotary speed was 300 rpm. The rotary power of RT by simulation was 51.82 kW, and the deviation between simulation and experiment was 6.36%.

The prediction of the power for CTSR and CTDR was given in Table 4. The prediction obtained that the draft power and rotary power of CTSR had a slightly reduction by that of CTDR. It was agreement with the field experiment. It indicated that the simulation could predict the experiment results qualitatively. However, the rotary power of CTSR and CTDR were only slightly less than that of RT, and the total power of CTSR and CTDR was larger than RT by simulation. The difference between the simulation and the measurement was possibly due to some of the complicated movement and force of soil in CTSR and CTDR that cannot be predicted by DEM model.

Table 4. The power characteristic of combined tillage implement by simulation.

Tillage Type	Draft Power (kW)	Rotary Power (kW)	Total Power (kW)
CTSR	5.53	47.20	52.73
CTDR	6.69	48.78	55.47

The effect of the forward speed and the rotary speed on power characteristics of RT and CTSR was given in Figure 7. The rotary power raised with the increase of the rotary speed and the forward speed for RT and CTSR. For CTSR, the draft power was only influenced by the forward speed and was not sensitive with the rotary speed. Compared the rotary power of RT and CTSR, their relationship was complicated. At a low forward speed (0.43 m/s), the rotary power of RT was less than that of CTSR with the rotary speed of 200 rpm but was larger than that of CTSR with the rotary speed of 300 rpm and 400 rpm. At a high forward speed (0.84 m/s), the rotary power of RT was less than that of CTSR with the rotary speed of 200 rpm and 300 rpm but was larger than that of CTSR with the rotary speed of 400 rpm. Though the simulation had not predicted the significant reduction of the rotary power with 0.43 m/s and 300 rpm, a similar reduction can be obtained with a relative higher rotary speed. The total power of CTSR was less than that of RT with 0.84 m/s and 400 rpm by simulation.

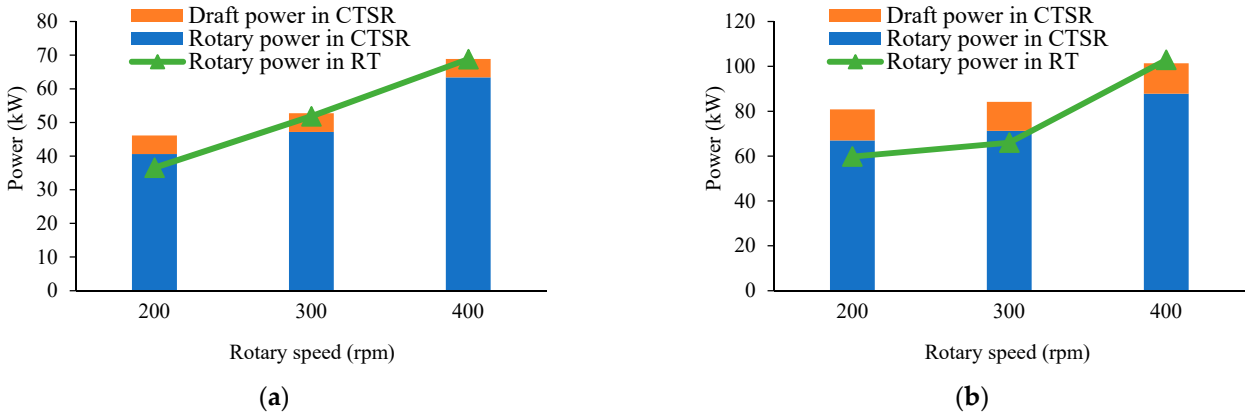

Figure 7. The effect of the forward speed and rotational speed on power: (**a**) forward speed = 0.43 m/s and (**b**) forward speed = 0.84 m/s.

4. Discussion

The performance indicators of combined tillage type (CTSR and CTDR) on straw incorporation were better than traditional rotary tillage type (RT). It revealed that the plough improved the performance of RT. A reasonable explanation was that the plough disturbed the original field before tillage by RT which made the tillage conditions of CTSR and CTDR were different with that of RT. Meanwhile, the total power consumption of combined tillage type (CTSR and CTDR) was smaller than other tillage types. It might be due to plough tillage made the soil loosen and reduced the cone index of the soil.

DEM simulation obtained the reduction of the rotary power in CTSR and CTDR compared with RT within the same operational parameters, but the degree of reduction was slightly. The total power of the combined tillage implement by simulation was even larger than RT. It was due to that the DEM model had not completely predicted the complicated soil–tool interaction. It was observed that the relationship of the rotary power of CTSR and RT in the simulation. The rotary power of CTSR was less than RT at some operational condition with a high rotary speed, and this contribution even can make the total power of CTSR less than that of RT. It demonstrated that the advantage of combined tillage implement on power consumption may be affected by the operational parameters.

The combined tillage implement can obtain an emission reduction at a relatively high rotary speed compared with RT.

The disturbance characteristics of CTSR and CTDR were not clear. DEM simulation was a promising method to study soil-tool interaction, and it could be used to investigate the disturbance characteristics of combined tillage type. The calculation consumption should be considered, as the diameter of soil particle for disturbance characteristics should be small enough. The straw was not considered in simulation in this manuscript. It should be involved to evaluate the effect of straw on the tillage tool disturbance characteristics. The reasonable straw model in DEM was a challenge for simulation.

5. Conclusions

Seven different tillage types were conducted in the rice field including a sole single-side plough (SP), a sole double-side plough (DP), a sole rotary tiller (RT), a two-pass tillage operation using a sole single-side plough followed by a sole rotary tiller (SP+RT), a two-pass tillage operation using a sole double-side plough followed by a sole rotary tiller (DP+RT), combined tillage implement of single-side plough and rotary tiller (CTSR), and combined tillage implement of double-side plough and rotary tiller (CTDR) to evaluate the performance of the combined tillage implement. The combined tillage implement (CTSR and CTDR) increased the ratio of straw coverage from 68.95% (RT) to appropriate 90%. With the help of the plough component, the combined tillage implement raised the stability coefficient of tillage depth. The surface evenness after tillage also improved with the comparison of RT. The combined tillage implement had an advantage on power requirement in the field experiment. Due to the reduction of the rotary power, the total power of the combined tillage implement was less than RT and two-pass tillage types. The DEM simulation predicted a slightly reduction of the rotary power, but the total power of the combined tillage implement was larger than RT with the same operational parameters. It was observed that the degree of the reduction on the rotary power was related to the operational parameters in the simulation. The effect of the operational parameters on the power requirement was also investigated by simulation, and the total power increased with the increase of the forward speed and rotary speed. The effect of working conditions on power consumption was investigated by DEM. The simulation was validated compared with rotary power of RT, and deviation between simulation and experiment was 6.36%. The reduction of the rotary power and the total power for CTSR was also obtained with specific working condition by simulation. The rotary power raised with the increase of the rotary speed and the forward speed for RT and CTSR, and the draft power was only influenced by the forward speed. As the soil–tool interaction was complicated and straw model was not involved, DEM simulation was not quantitatively predicted the field experiment results. There were some differences on the degree of power reduction by DEM simulation and field experiment. The disturbance characteristics of different tillage implements with considering straw model was still a challenge in DEM simulation.

6. Patents

Combined tillage implement with plough and rotary tiller in dry field (Patents No.: CN20190753529.6).

Author Contributions: Conceptualization, J.D. and J.X.; methodology, J.D., Y.H. and W.Z.; software, Y.H.; validation, K.Z. and J.Z.; formal analysis, J.D.; investigation, J.D.; resources, J.X.; data curation, J.D. and Y.H.; writing—original draft preparation, J.D. and Y.H.; writing—review and editing, J.X.; visualization, Y.H.; supervision, J.X.; project administration, J.D. and J.X.; funding acquisition, J.D. and J.X. All authors have read and agreed to the published version of the manuscript.

Funding: This work was funded by the Natural Science Foundation of Hubei province (No. 2020CFB143), and the National Key Technology R&D Program (grant number 2017YFD0301300).

Institutional Review Board Statement: Not applicable.

Informed Consent Statement: Not applicable.

Data Availability Statement: Data sharing not applicable.

Conflicts of Interest: The authors declare no conflict of interest.

References

1. Zhou, H.; Zhang, C.; Zhang, W.; Yang, Q.; Li, D.; Liu, Z.; Xia, J.F. Evaluation of straw spatial distribution after straw incor-poration into soil for different tillage tools. *Soil Tillage Res.* **2020**, *196*, 104440. [CrossRef]
2. Chen, Y.; Monero, F.V.; Lobb, D.; Tessier, S.; Cavers, C. Effects of sex tillage methods on residue incorporation and crop per-formance in a heavy clay soil. *Trans. ASAE* **2020**, *47*, 1003–1010. [CrossRef]
3. Lee, K.; Park, S.; Park, W.; Lee, C. Strip tillage characteristics of rotary tiller blades for use in a dryland direct rice seeder. *Soil Tillage Res.* **2003**, *71*, 25–32. [CrossRef]
4. Saimbhi, V.; Wadhwa, D.; Grewal, P. Development of a Rotary Tiller Blade using Three-dimensional Computer Graphics. *Biosyst. Eng.* **2004**, *89*, 47–58. [CrossRef]
5. Asl, J.H.; Singh, S. Optimization and evaluation of rotary tiller blades: Computer solution of mathematical relations. *Soil Tillage Res.* **2009**, *106*, 1–7. [CrossRef]
6. Matin, A.; Fielke, J.M.; Desbiolles, J. Furrow parameters in rotary strip-tillage: Effect of blade geometry and rotary speed. *Biosyst. Eng.* **2014**, *118*, 7–15. [CrossRef]
7. Matin, M.; Fielke, J.; Desbiolles, J. Torque and energy characteristics for strip-tillage cultivation when cutting furrows using three designs of rotary blade. *Biosyst. Eng.* **2015**, *129*, 329–340. [CrossRef]
8. Matin, M.; Desbiolles, J.; Fielke, J. Strip-tillage using rotating straight blades: Effect of cutting edge geometry on furrow parameters. *Soil Tillage Res.* **2016**, *155*, 271–279. [CrossRef]
9. Ucgul, M.; Saunders, C.; Li, P.; Lee, S.H. Analyzing the mixing performance of a rotary spader using digital image pro-cessing and discrete element modelling (DEM). *Comput. Electron. Agric.* **2018**, *151*, 1–10. [CrossRef]
10. Li, S.; Chen, X.; Chen, W.; Zhu, S.; Li, Y.; Yang, L.; Xie, S.; Yang, M. Soil-cutting simulation and parameter optimization of handheld tiller's rotary blade by Smoothed Particle Hydrodynamics modelling and Taguchi method. *J. Clean. Prod.* **2018**, *179*, 55–62. [CrossRef]
11. Ahmadi, I. A power estimator for an integrated active-passive tillage machine using the laws of classical mechanics. *Soil Tillage Res.* **2017**, *171*, 1–8. [CrossRef]
12. Upadhyay, G.; Raheman, H. Performance of combined offset disc harrow (front active and rear passive set configuration) in soil bin. *J. Terramechanics* **2018**, *78*, 27–37. [CrossRef]
13. Upadhyay, G.; Raheman, H. Effect of velocity ratio on performance characteristics of an active-passive combination tillage implement. *Biosyst. Eng.* **2020**, *191*, 1–12. [CrossRef]
14. Usaborisut, P.; Prasertkan, K. Performance of combined tillage tool operating under four different linkage configurations. *Soil Tillage Res.* **2018**, *183*, 109–114. [CrossRef]
15. Usaborisut, P.; Prasertkan, K. Specific energy requirements and soil pulverization of a combined tillage implement. *Heliyon* **2019**, *5*, e02757. [CrossRef]
16. Shmulevich, I. State of the art modeling of soil–tillage interaction using discrete element method. *Soil Tillage Res.* **2010**, *111*, 41–53. [CrossRef]
17. Ucgul, M.; Saunders, C. Simulation of tillage forces and furrow profile during soil-mouldboard plough interaction using dis-crete element modelling. *Biosyst. Eng.* **2020**, *190*, 58–70. [CrossRef]
18. Johnson, K.L.; Kendall, K.; Roberts, A.D. Surface energy and the contact of elastic solids. *Proc. R. Soc. Lon. Ser. A* **1971**, *324*, 301–313.
19. Du, J.; Xia, J.; Wu, H.; Xu, W. An Investigation of the Performance of Waterjet for Lotus Root Digging Device: Simulation and Experiment. *Int. J. Fluid Mach. Syst.* **2020**, *13*, 160–166. [CrossRef]
20. Zhang, X.M. Study on Working Mechanism and Experimental of Rotary Tiller for High Straw Returning. Ph.D. Thesis, Huazhong Agricultural University, Wuhan, China, 2017.
21. Coetzee, C.J. Review: Calibration of the discrete element method. *Powder Technol.* **2017**, *310*, 104–142. [CrossRef]